Symmetrical Triangular LFM for Underwater Acoustic Communications

Qiaosong Cai, Fei Yuan*, Jianghui Li†, Chunxian Gao, Ben Roche‡
Key Laboratory of Underwater Acoustic Communication and Marine Information Technology,
Ministry of Education, Xiamen University, China
†Institude of Sound and Vibration Research, University of Southampton, Southampton SO17 1BJ, U.K.
‡Ocean and Earth Science, University of Southampton, National Oceanography Centre, Southampton SO14 3ZH, U.K.
E-mail: yuanfei@xmu.edu.cn

***Abstract*—Synchronous detection acts as a key role in underwater acoustic communications. It is discovered that the Symmetrical Triangular Linear Frequency Modulation (STLFM) signal has double energy peaks in their fractional Fourier transform domain and these two peaks have symmetry in their amplitude if the STLFM signal is captured in the accurate time windows for the synchronization. In this paper, we propose a synchronization detection method based on the STLFM. To verify the effectiveness of the proposed method, we apply simulations based on the Bellhop program and sea trial data collected at Wuyuan Bay, Xiamen, China. The results show that the proposed STLFM method outperforms the LFM method.**

***Index Terms*—underwater acoustic communications (UAC), Symmetrical Triangular Linear Frequency Modulation (STLFM), synchronization**

I. Introduction

Underwater acoustic channel is complex in time, space, and frequency [1]–[10]. It is often characterized as time-varying, multipath, and limited bandwidth [11]–[13], which distort acoustic signals seriously in the channel. Therefore, the performance of underwater acoustic communications (UAC) largely depends on the synchronization detection. In practical applications, both communication and positioning system require high accuracy and stability of synchronization. Currently, methods for improving the performance of synchronization, include signal structure design and signal processing [14].

Linear frequency modulation (LFM) has been well performed and widely used in UAC due to its autocorrelation property and pulse pressure characteristics [15]–[17]. Most of the existing underwater acoustic synchronization signals are based on the LFM signal or its extended signals [14], [18], [19]. Among these signals, symmetrical triangular linear frequency modulation (STLFM) [7] is one of the preferred synchronization signal at low signal-to-noise ratio (SNR) due to its large time bandwidth product and symmetrical triangular structure [20], [21].

This paper is organised as follows. Section II describes the STLFM signal. Sections III describes the synchronization algorithm. Section IV compares the proposed algorithm and the existing LFM algorithm using the Bellhop simulation and field data. Section V summarizes the paper.

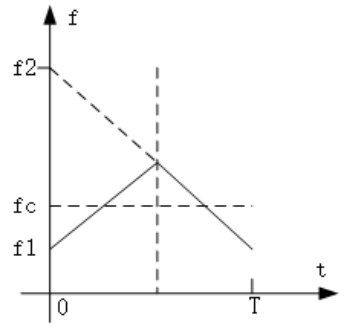

Fig. 1. Diagram of the Symmetrical Triangular Linear Frequency Modulation (STLFM).

II. STLFM synchronization signal

Each period of the STLFM signal S_T includes two parts of the positive frequency modulation $S_T^+(t)$ and negative frequency modulation $S_T^-(t)$. Assume that the period of STLFM signal is T, and its frequency first in the first half period [0, T/2] linearly rises to a certain value, then linearly drops to the starting value in the second half of the period [T/2, T], expressed as

$$S_T^+(t) = A\exp\left\{j2\pi\left[\left(f_c - \frac{\mu T}{4}\right)t + \frac{\mu t^2}{2}\right] + j\phi_1\right\}, \quad (1)$$

and

$$S_T^-(t) = A\exp\left\{j2\pi\left[\left(f_c + \frac{\mu T}{4}\right)\left(t - \frac{T}{2}\right) - \frac{\mu\left(t - \frac{T}{2}\right)^2}{2}\right] + j\phi_2\right\}, \quad (2)$$

where A is the signal amplitude, T is the sweep period, f_c is the effective center frequency of the signal, μ is the modulation frequency, ϕ_1 and ϕ_2 are the initial phases, and $\phi_2 = \pi f_c T + \phi_1$. Fig. 1 shows the schematic diagram of the STLFM signal. In the figure, f_1 and f_2 are the equivalent initial frequencies of the upper and lower frequency modulation parts. Fig. 2 shows two peaks in the fractional Fourier transform (FRFT) domain. The bimodal position and symmetry axis are in the ideal case.

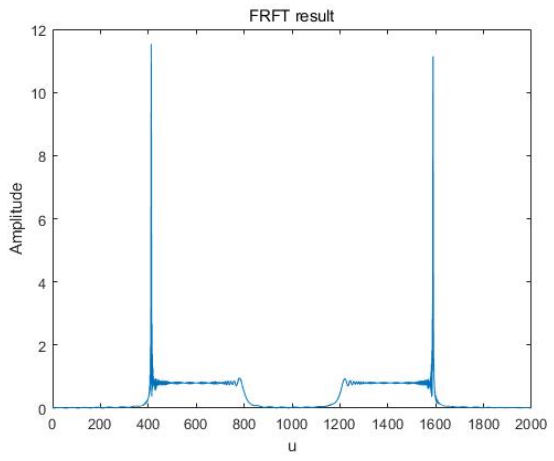

Fig. 2. STLFM in the fractional Fourier transform (FRFT) domain.

Using FRFT for the signal and supposing the upper Frequency Modulation (FM) transformation, the peaks position μ_1 and μ_2 can be given by

$$\mu_1 = \left(f_c - \frac{\mu T}{4}\right)\sin\alpha, \tag{3}$$

$$\mu_2 = \left(f_c + \frac{3\mu T}{4}\right)\sin\left(-\alpha\right), \tag{4}$$

where α is the angle, and f_c is the center frequency. The position of the peaks is related to the starting frequency and FRFT transformation angle, use Eq.(3) minus Eq.(4), we obtain

$$|\mu_2 - \mu_1| = \left(2f_c + \frac{\mu T}{2}\right)\sin\alpha = 2F\sin\alpha, \tag{5}$$

where F is the maximum frequency within the bandwidth. It can be seen that the STLFM obtains two peaks with different positions through FRFT transformation, and the spacing between the two peaks is related to its maximum frequency and the current FRFT transformation angle. Considering the time delay and the frequency shift caused by the complex channel, with the delay and the frequency characteristics of FRFT, the peaks position μ_{1r} and μ_{2r} can be given by

$$\mu_{1r} = \mu_1 - \tau\cos\alpha - \varepsilon\sin\alpha, \tag{6}$$

$$\mu_{2r} = \mu_2 - \tau\cos\left(-\alpha\right) - \varepsilon\sin\left(-\alpha\right), \tag{7}$$

where τ is the time delay, and ε is the frequency shift. Thus, when the received signal is delayed, the symmetry axis position is offset, which has a certain relationship with τ.

III. Synchronization algorithm

The STLFM synchronization algorithm can be obtained based on the symmetry axis. Such synchronization algorithms incorporates two steps: synchronization capture, and synchronization tracking.

A. Synchronization capture based on symmetry axis correction

To achieve synchronization capture, we first make a correction to pull the signal and FRFT transform window to a relatively close position. It avoids too much peak attenuation of the direct path signal and reduces the amount of computation for subsequent synchronization processing. Then, the effects of Doppler spread are compensated for achieving better FRFT spike.

According to Eq.(6) and Eq.(7), the symmetry axis positions of the double peaks are:

$$\frac{(\mu_{2r} + \mu_{1r})}{2} = \frac{(\mu_{2r} + \mu_{1r})}{2} - \tau\cos\alpha, \tag{8}$$

where μ_{1r} and μ_{2r} represent the bimodal positions affected by the delay.

As discussed above, the symmetry axis is affected by τ rather than ε. The ε has been offset by the Doppler shift of upper and lower FM. The symmetry axis of the initial FRFT result of the received signal is subtracted from the original symmetry axis parameter to obtain the delay τ. Then the τ can be given by

$$\tau = \frac{\left[\frac{(\mu_{2r}+\mu_{1r})}{2} - \frac{(\mu_2+\mu_1)}{2}\right]}{\cos\alpha}. \tag{9}$$

The position of the synchronization window can be corrected by τ. Supposing the Doppler factor of the existing Doppler spread is D, and the maximum frequency becomes DF. Since the Doppler spread has little effect on the optimal order, the original order FRFT transform does not lose its energy focusing characteristics. The FRFT bimodal spacing after Doppler expansion is

$$|\mu_{2\varepsilon} - \mu_{1\varepsilon}| = 2DF\sin\alpha, \tag{10}$$

where $\mu_{1\varepsilon}$ and $\mu_{2\varepsilon}$ represent the bimodal positions affected by Doppler. The Doppler factor D is found by Eq.(5) and Eq.(10) to adjust the optimal FRFT transformation order to

$$p' = -\frac{2}{\pi}\operatorname{arccot} D^2\mu. \tag{11}$$

It also adjusts the FRFT transform window length to the T/D of the current STLFM cycle length.

B. Synchronization tracking based on peak difference correction

After the symmetry axis is corrected, there will still be energy overflow due to the small difference of the synchronization position. At this time, the double peak of the FRFT domain will have a high and low difference, and the synchronization tracking loop can be used to accurately track the signal. The synchronization tracking loop is a closed-loop processing structure for the purpose of "locking the bimodal amplitude difference below the preset threshold", and estimating the synchronization deviation by the bimodal amplitude difference, without setting an absolute threshold.

The closed loop synchronization tracking procession is shown in the Fig. 3. Step A performs an order-corrected FRFT

transform on the signal after the symmetric axis synchronization correction, and takes the double peak maximum value $|R_{m1}|^2$, $|R_{m2}|^2$. Then we calculate the threshold R. If R is greater than the preset value m, the synchronization window moves τ ($\tau = T/f_s$, T is the STLFM signal period, and F_s is the sampling rate), and repeats the first step to perform the next synchronization tracking procession until R is less than the preset value m, which indicates that the peak amplitude difference has been controlled within an acceptable range. At this time, the FRFT bimodal amplitudes are nearly equal, meaning that the synchronization is successful.

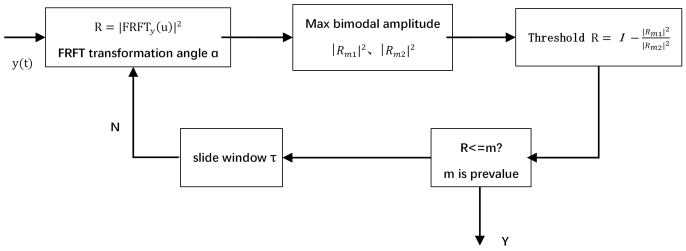

Fig. 3. Block diagram of synchronous tracking process.

IV. Numerical Results

We compare and verify the LFM synchronization algorithm based on a single peak position in FRFT domain with the proposed STLFM synchronization algorithm. The frequency range of LFM and STLFM signal is from 20 kHz to 30 kHz, the duration is 20 ms, and the system sampling rate is 100 kHz.

The algorithm is tested for several times. The error between the synchronization position and the ideal value (synchronization error) obtained by each test is statistically analysed in terms of histogram and error distribution probability. Then, the performance of the LFM synchronization algorithm and the STLFM synchronization algorithm are compared. The histogram form highlights the stability of the synchronization of the two algorithms, and the error distribution probability can directly reflect the difference in synchronization accuracy between the two algorithms.

A. Bellhop simulation

In Bellhop simulation, the transmission distance is 1000 m, and the transducer depth is 10 m. As shown in Fig. 4(a), the channel has 6-path impulse response. Fig. 4(b) shows the amplitude of the received signal which is significantly jittery in the time-domain.

The synchronization errors of the two algorithms are counted as shown in TABLE I. The mean square error (MSE) reflects the stability of synchronization. The MSE of the STLFM synchronization algorithm in this paper is reduced to 1/20 of the LFM synchronization algorithm.

As shown in Fig. 5, the synchronization errors of the STLFM algorithm is concentrated in [-0.01,0.01] while the LFM is concentrated in [-0.03,0.03]. Therefore, the STLFM algorithm is relatively more stable. As shown in Fig. 6, most of the synchronization error of the LFM algorithm are uniformly

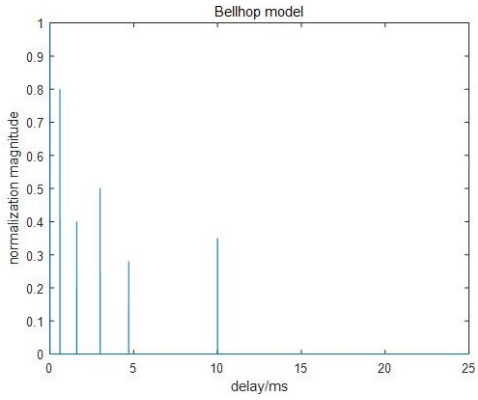

(a) Bellhop multipath model

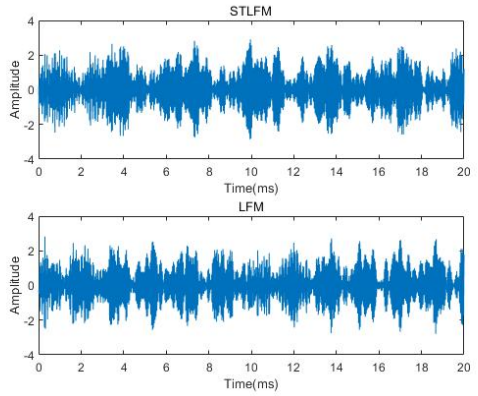

(b) Received signals

Fig. 4. Bellhop multipath model and received signals.

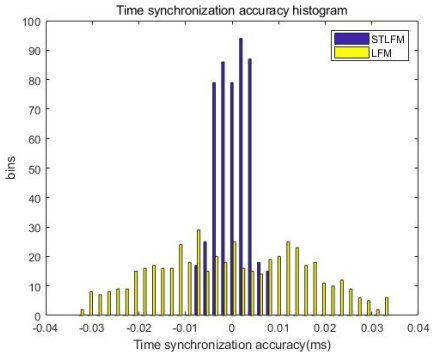

Fig. 5. Synchronization error histogram.

TABLE I
MSE Statistics of Bellhop Model and Wuyuanwan Channel

Algorithm \ MSE(ms^2)	Bellhop model	Wuyuanwan channel
LFM	2.4195e-04	2.3001e-03
STLFM	1.2750e-05	4.1001e-04

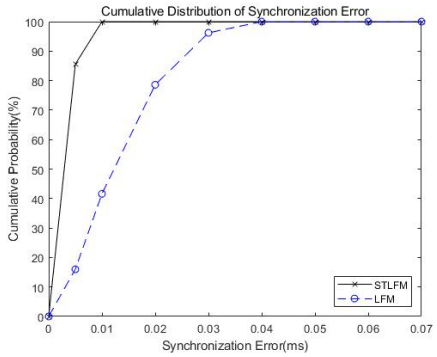

Fig. 6. Error distribution probability.

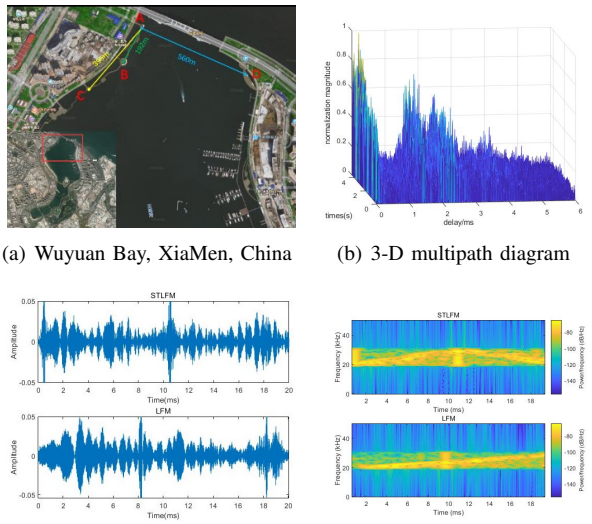

(a) Wuyuan Bay, XiaMen, China (b) 3-D multipath diagram

(c) Receive signals (d) Time-frequency diagram

Fig. 7. Multipath channel and received signals collected in Wuyuan Bay, Xiamen, China [7].

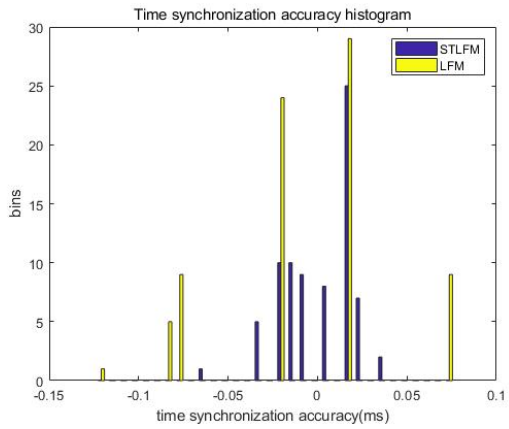

Fig. 8. Synchronization error histogram

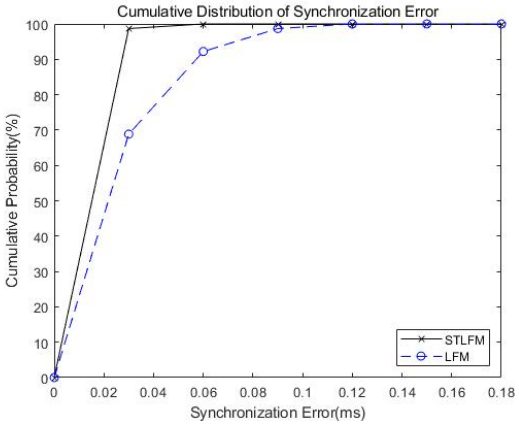

Fig. 9. Error distribution probability

distributed in the range of 0.04 ms, only 42% of them are in the range of 0.01 ms. While the synchronization errors of the STLFM algorithm are mostly in the range of 0.01 ms, and about 86% of them are in the range of 0.005 ms. Therefore, the synchronization performance of STLFM algorithm is better than that of the LFM.

B. Field channel experiment

Further comparison of LFM and STLFM synchronization algorithms is performed in Wuyuan Bay, Xiamen, China. The test scenario is shown in Fig. 7(a). The signal was transmitted at point A and was received at point D. Fig. 7(b) shows a three-dimensional (3-D) multipath diagram during the test. The X-axis is the multipath delay, the Y-axis is the time, and the Z-axis is the normalized channel impulse response. Fig. 7(c) shows the time domain waveform of the received signal with large distortion. Fig. 7(d) shows the time-frequency spectrum, which indicates that the received signal suffers from significant multipath and background noise.

Fig. 8 shows the synchronization error histogram distribution of the actual underwater channel which is more dispersed than the Bellhop simulation channel. Despite this, the synchronization error of the STLFM algorithm is obviously concentrated in a smaller range of [0.065,0.036], while the LFM algorithm is concentrated in [-0.12,0.07], which indicates its anti-multipath performance.

The MSE of the synchronization algorithm is reduced to 1/5 of the LFM synchronization algorithm. As shown in Fig. 9, most of the synchronization errors of the LFM algorithm are uniformly distributed in the range of 0.12 ms, only 69% of them are in the range of 0.03 ms. While the synchronization errors of the proposed STLFM algorithm are mostly in the range of 0.06 ms, about 99% of them are in the range of 0.03 ms.

V. Conclusion

In this paper, symmetrical triangular linear frequency modulation (STLFM) is used as the synchronization signal of underwater acoustic communications. Using the symmetry of STLFM in time domain and FRFT domain to realize synchronization tracking. Compared to the LFM synchronous acquisition and tracking method, the use of STLFM's bimodal relative relationship on the FRFT domain translates

the detection of absolute peaks into the detection of relative peak, thereby it can better adapt to the changing channel environments. Through Bellhop simulation and a large number of sea-test data, the STLFM synchronization algorithm achieves better stability and accuracy than the traditional LFM synchronization algorithm in the same condition of the same time-bandwidth.

ACKNOWLEDGMENT

Funding for this work was partly provided by the National Natural Science Foundation of China (61571377, 61771412, 61871336) and the Fundamental Research Funds for the Central Universities (20720180068), and partly provided by the European Unions Horizon 2020 research and innovation programme under the grant agreement number 654462 (STEMM-CCS).

REFERENCES

[1] J. Li, L. Liao, and Y. V. Zakharov, "Space-time cluster combining for UWA communications," in *IEEE OCEANS 2016-Shanghai*, 2016, pp. 1–6.

[2] J. Li and Y. V. Zakharov, "Efficient use of space-time clustering for underwater acoustic communications," *IEEE Journal of Oceanic Engineering*, vol. 43, no. 1, pp. 173–183, 2018.

[3] J. Li, Y. V. Zakharov, and B. Henson, "Multibranch Autocorrelation Method for Doppler Estimation in Underwater Acoustic Channels," *IEEE Journal of Oceanic Engineering*, vol. 43, no. 4, pp. 1099 – 1113, 2018.

[4] J. Li and Y. V. Zakharov, "Sliding-window homotopy adaptive filter for estimation of sparse UWA channels," in *IEEE 9th Sensor Array and Multichannel Signal Processing Workshop (SAM), Rio de Janeiro, Brazil*, 2016, pp. 1–4.

[5] J. Li, "DOA tracking in time-varying underwater acoustic communication channels," in *MTS/IEEE OCEANS 2017-Aberdeen, UK*, 2017, pp. 1–9.

[6] J. Li and Y. V. Zakharov, "Sliding window adaptive filter with diagonal loading for estimation of sparse UWA channels," in *IEEE OCEANS 2016-Shanghai, China*, 2016, pp. 1–5.

[7] F. Yuan, Z. Jia, J. Li, and E. Cheng, "STLFM Signal Based Adaptive Synchronization for Underwater Acoustic Communications," *IEEE Access*, vol. 7, pp. 28 734–28 748, 2019.

[8] Y. Zhang, T. Wu, Y. Zakharov, and J. Li, "MMP-DCD-CV based sparse channel estimation algorithm for underwater acoustic transform domain communication system," *Applied Acoustics*, vol. 154, pp. 43–52, 2019.

[9] Y. Zhang, J. Li, Y. Zakharov, X. Li, and J. Li, "Deep learning based underwater acoustic OFDM communications," *Applied Acoustics*, vol. 154, pp. 53–58, 2019.

[10] J. Li, P. R. White, J. M. Bull, and T. G. Leighton, "A noise impact assessment model for passive acoustic measurements of seabed gas fluxes," *Ocean Engineering*, vol. 183, no. 1, pp. 294–304, 2019.

[11] M. Stojanovic, "Recent advances in high-speed underwater acoustic communications," *IEEE Journal of Oceanic engineering*, vol. 21, no. 2, pp. 125–136, 1996.

[12] I. F. Akyildiz, D. Pompili, and T. Melodia, "Challenges for efficient communication in underwater acoustic sensor networks," *ACM Sigbed Review*, vol. 1, no. 2, pp. 3–8, 2004.

[13] M. Stojanovic, "Underwater acoustic communication," *Wiley Encyclopedia of Electrical and Electronics Engineering*, pp. 1–12, 1999.

[14] M. Stojanovic, J. A. Catipovic, and J. G. Proakis, "Phase-coherent digital communications for underwater acoustic channels," *IEEE journal of oceanic engineering*, vol. 19, no. 1, pp. 100–111, 1994.

[15] P. A. Van Walree and R. Otnes, "Ultrawideband underwater acoustic communication channels," *IEEE Journal of Oceanic Engineering*, vol. 38, no. 4, pp. 678–688, 2013.

[16] B. Li, J. Huang, S. Zhou, K. Ball, M. Stojanovic, L. Freitag, and P. Willett, "MIMO-OFDM for high-rate underwater acoustic communications," *IEEE Journal of Oceanic Engineering*, vol. 34, no. 4, pp. 634–644, 2009.

[17] S. Roy, T. M. Duman, V. McDonald, and J. G. Proakis, "High-rate communication for underwater acoustic channels using multiple transmitters and space–time coding: Receiver structures and experimental results," *IEEE Journal of Oceanic Engineering*, vol. 32, no. 3, pp. 663–688, 2007.

[18] S. F. Mason, C. R. Berger, S. Zhou, and P. Willett, "Detection, synchronization, and doppler scale estimation with multicarrier waveforms in underwater acoustic communication," *IEEE Journal on selected areas in communications*, vol. 26, no. 9, pp. 1638–1649, 2008.

[19] F. Wei, X. Xiaomei, Z. Lan, and C. Yougan, "A frame synchronization method for underwater acoustic communication on mobile platform," in *2010 International Conference on Image Analysis and Signal Processing*. IEEE, 2010, pp. 518–522.

[20] Q. Liu, Y. Luo, S. Gao *et al.*, "Multi-target parameter estimation in symmetry triangular LFMCW radar based on envelope compensation," *Acta Eletronica Sinica*, vol. 44, no. 3, pp. 541–547, 2016.

[21] T. Jiang, Z. Yongjun, and Y. Kun, "New method for detection and parameter estimation of STLFM signal," in *IET International Radar Conference 2013*, 2013, pp. 1–7.